



Preparation of a mesoporous silica-based nano-vehicle for dual DOX/CPT pH-triggered delivery

Maria C. Llinàs^{a*}, Gabriel Martínez-Edo^{a*}, Anna Cascante^a, Irene Porcar^a, Salvador Borrós^{a,b}  and David Sánchez-García^a 

^aGrup d'Enginyeria de Materials (GEMAT), Institut Químic de Sarrià, Universitat Ramon Llull, Barcelona, Spain; ^bCentro de Investigación Biomédica en Red en Bioingeniería, Biomateriales y Nanomedicina (CIBER-BBN), Zaragoza, Spain

ABSTRACT

A dual doxorubicin/camptothecin (DOX/CPT) pH-triggered drug delivery mesoporous silica nanoparticle (MSN)-based nano-vehicle has been prepared. In this drug-delivery system (DDS), CPT is loaded inside the pores of the MSNs, while DOX is covalently attached to the surface of an aldehyde-functionalized MSN through a dihydrazide–polyethylene glycol chain. Thus, DOX and the linker act as pH-sensitive gatekeeper. The system is versatile and easy to assemble, not requiring the chemical modification of the drugs. While at physiological conditions the release of the drugs is negligible, at acidic pH a burst release of DOX and a gradual release of CPT take place. In vitro cytotoxicity tests have demonstrated that this DDS can deliver efficiently DOX and CPT for combination therapy.

ARTICLE HISTORY

Received 23 March 2018
Revised 24 April 2018
Accepted 1 May 2018

KEYWORDS

Mesoporous silica nanoparticles; dual release; doxorubicin; camptothecin; combination therapy

1. Introduction



Despite the encouraging progress in tumor biology and chemotherapy, adequate cancer treatment is far from satisfactory. The therapeutic effect of chemotherapy remains quite poor due to insufficient drug dosage to the diseased regions, rapid blood clearance, severe side effects and drug resistance (Siegel et al., 2015). One promising strategy to address these drawbacks is the use of multifunctional drug-delivery systems (DDSs), including micelles, drug conjugates, as well as polymeric and inorganic nanoparticles (Rosenholm et al., 2010; Rosenholm et al. 2011; Wang et al., 2012; Choi et al., 2012).

In this context, mesoporous silica nanoparticles (MSNs) present outstanding properties for drug delivery applications (Trewyn et al., 2007; Coti et al., 2009; Mai & Meng, 2013; Argyo et al., 2014) owing to their good biocompatibility, (Mamaeva et al., 2013) easy chemical modification (Khung & Narducci, 2015) and high encapsulation capacity (Martínez-Carmona et al., 2015). This chemical versatility opens the door to the design of stimuli-responsive DDS, which allows selective release of the payload, (Wang et al., 2009; Kamarudin et al., 2013; Natarajan & Selvaraj, 2014) by means of smart gates installed at the external surface of the nanoparticle (Choi et al., 2012; Li et al., 2012; Argyo et al., 2014; Martínez-Carmona et al., 2015; Song & Yang, 2015). Among them, pH-triggered systems promise to be one of the most powerful tools in the development of smart nanocapsules for cancer applications (Gao et al., 2010; Lee et al., 2010, 2011;


Fan et al., 2011; Kar et al., 2013; Yang et al., 2014; Li et al., 2015b) due to the difference of pH between tumor and normal tissues (Vivero-Escoto et al., 2010; Yang et al., 2014).

All these features endow MSN with ideal properties to design DDS for the co-delivery of anticancer drugs, which is the basis of the so-called combination chemotherapy (Shah & Schwartz, 2000; Miles et al., 2002). The general principle of combination therapy is the administration of more than one drug, with independent mechanism of action, with the aim to enhance the efficiency of the treatment. This approach has been proposed for the treatment of aggressive brain tumors such as glioblastoma (Kim et al., 2013; Nonnenmacher et al., 2015).

To this end, DDS for the combined release of chemotherapeutic agents using MSNs for cancer have been described (Li et al., 2013; Muhammad et al., 2014; Wang et al., 2014b). In particular, the combination of camptothecin (CPT) with doxorubicin (DOX) has attracted great interest due to their potent inhibition of enzymes topoisomerase I and II, respectively, leading to a synergistic chemotherapy (Pavillard et al., 2001; Camacho et al., 2015). Examples of such DDS have been recently reported (Li et al., 2013; Muhammad et al., 2014; Zhou et al., 2015). However, the preparation of these systems is still complex and entails the assembly of many different components [i.e. macrocycles (Zhou et al., 2015) quantum dots (Muhammad et al., 2014; Li et al. 2015b)] or the derivatization of the drug (Li et al., 2013). As a consequence, this

CONTACT David Sánchez-García  david.sanchez@iqs.edu  Grup d'Enginyeria de Materials (GEMAT), Institut Químic de Sarrià, Universitat Ramon Llull, Barcelona, Spain

*These authors contributed equally to this work.

 Supplemental data for this article can be accessed [here](#).

© 2018 The Author(s). Published by Informa UK Limited, trading as Taylor & Francis Group.

This is an Open Access article distributed under the terms of the Creative Commons Attribution-NonCommercial License (<http://creativecommons.org/licenses/by-nc/4.0/>), which permits unrestricted non-commercial use, distribution, and reproduction in any medium, provided the original work is properly cited.

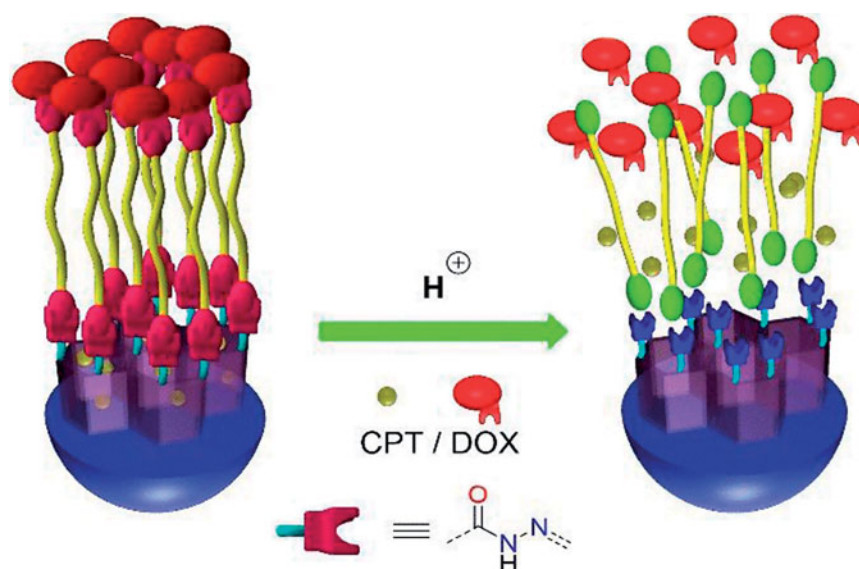


Figure 1. Proposed DDS for dual drug release.

complexity could hamper the practical use of these DDS. Furthermore, the design of effective gates to avoid the premature leakage of the cargo is still a challenge (Li et al., 2013, 2015b).

Herein, we report on the preparation of a pH-responsive DDS based on MSNs for dual drug delivery (CPT@MSN-hyd-PEG-hyd-DOX, hyd = hydrazone group), in particular CPT and DOX. In this DDS, CPT is loaded into the pores of the MSNs, while DOX is covalently attached to the surface of an aldehyde-functionalized MSN through a dihydrazone–polyethylene glycol chain. Thus, DOX and the linker act as pH-sensitive gatekeeper, which effectively blocks the release of CPT at neutral pH (Figure 1) (Zhao et al., 2009).

Therefore, the proposed nano-vehicle presents the following features: (a) the system can be easily prepared in a three-step procedure (b) both CPT and DOX are not chemically derivatized, what simplifies the preparation of the carrier (Schmid et al., 2007; Shen et al., 2010; Li et al., 2013; Xu et al., 2015a) (c) the system is potentially useful as a general nano-platform for many drug combinations, (d) the hydrazone linker assures the selective release of both DOX and CPT triggered by the acidic environment of the tumor, avoiding any premature leakage (Li et al., 2013) (e) the modular design allows the decoration of the MSN with additional imaging probes or targeting ligands.

2. Materials and methods

2.1. Materials and measurements

Cetyltrimethylammonium bromide (CTAB), tetraethylorthosilicate (TEOS), and 3-aminopropyl triethoxysilane (APTES) were purchased from ACROS; Ammonium hydroxide solution (5M) and methylene blue from Fluka; CPT from Apollo; 2,2-dimethoxyethan-1-amine, hydrazine hydrate, tetraethylene glycol and DOX hydrochloride from Sigma-Aldrich. All the chemicals were used as received without further purification.

2.2. Instruments

TEM microscopy was carried out using a JEOL microscope model JEM 2011 in Universitat Autònoma de Barcelona (UAB). Bio-TEM microscopy of HeLa cells was performed using a JEOL microscope model JEM-1400 in Universitat Autònoma de Barcelona (UAB). Fluorescence confocal microscopy was carried out using a multiphoton spectral Leica model TCS SP5 (UAB). Uptake kinetic experiments were carried out using an IncuCyte[®] S3 Live-cell Analysis System (Essen Bioscience, Ann Arbor, MI). Porous surface nitrogen physisorption analysis was conducted on a Micromeritics Gemini V surface area and pore size analyzer. Pore size distribution curves were obtained from analysis of the absorption portion of the isotherms using the BJH (Barrett–Joyner–Halenda) method. Dynamic light scattering (DLS) size and ζ -potential measurements were obtained using a Malvern Zetasizer Nano Series ZEN 3600. Small angle powder X-ray diffraction (SXRD) were performed with a Philips X'Pert diffractometer equipped with Cu K α radiation (wavelength 1.5406 Å) at 'Centro de asistencia a la investigación de rayos X de la Universidad Complutense de Madrid'. XRD patterns were collected in the 2θ range between 0.6° and 6.5° with a step size of 0.02° and counting time of 5 s per step. Infrared Spectra (FTIR) was recorded on a Thermo Scientific Nicolet iS10 FTIR spectrometer with Smart iTr. Values were reported in wavenumbers (cm⁻¹). The notation used was KBr (potassium bromide plates) and film (evaporated film from chloroform). Organic combustion elemental analysis (OEA) were performed in a EuroVector Instruments Euro EA elemental analyzer. UV–vis absorption and fluorescence spectra were recorded using a Thermo Scientific 300 UV–vis spectrophotometer. Fluorescence excitation spectra were recorded on a Hitachi F2500 fluorescence spectrophotometer. FACS analysis was performed using a flow cytometer (BD LSR Fortessa) at IGTP ('Institut d'Investigació Germans Trias i Pujol').

2.3. Synthesis of MSN-(NH₂) CTAB

Tetraethylorthosilicate in EtOH (1.6 mL, 0.2 M) was added dropwise to a solution of CTAB (0.2 g) in NH_{3(aq)} (0.5 M, 100 mL) at 60 °C. Then, the resulting mixture was stirred for 5 h. Subsequently, APTES in EtOH (1.6 mL, 12% v/v) and TEOS in EtOH (1.6 mL, 1 M) were added dropwise. This solution was stirred at the same temperature for another 1 h. Finally, the mixture was aged for 24 h. Solid samples were collected via centrifuging, washing and dispersing with deionized H₂O.

2.4. Synthesis of MSN-(NH₂)_i(CHO)_o

MSN-(NH₂) CTAB (0.2 g) were reacted with 4 eq. of 2-isothiocyanate-1,1-dimethoxyethane (**1**) (0.1 g, 6.8·10⁻⁴ mol) in 50 mL of toluene. After 24 h, MSNs were washed twice with toluene and ethanol. Then, the tensioactive was removed by treatment of MSN-(NH₂)_i(Acet)_o with an ethanolic solution (40 mL) of NH₄NO₃ (0.5 g) (25 °C). After 24 h, MSNs were washed with EtOH and the acetal protecting group was removed by stirring MSNs in 30 mL of 0.1 M HCl for 6 h.

2.5. Synthesis of MSN-hyd-PEG-hyd-DOX

To MSN-(NH₂)_i(CHO)_o (30 mg) in MeOH (30 mL) a solution of dihydrazide-PEG **2** (0.080 g, 2.36·10⁻⁴ mol) in MeOH (20 mL) was added. Then, after 48 h, MSNs were centrifuged, washed with MeOH and the supernatant was collected. Afterward, DOX (21 mg, 3.6·10⁻⁵ mol) was added to the resulting MSNs suspended in MeOH (20 mL). Finally, after 48 h MSNs were washed with MeOH (three times) and H₂O (three times), until no red supernatant was obtained and then lyophilized. DOX loading was quantified by UV-vis spectroscopy (490 nm) from the supernatant.

2.6. Synthesis of CPT@MSN-hyd-PEG-hyd-DOX

Camptothecin (18 mg, 5.16·10⁻⁵ mol) was dissolved in CHCl₃ (35 mL) with the aid of sonication at 60 °C until total dissolution of the drug was achieved. Then, CPT solution was added to a stirred suspension of MSN-(NH₂)_i(CHO)_o (30 mg) in MeOH (25 mL) (700 rpm, 23 °C). Afterwards (24 h), a solution of dihydrazide-PEG **2** (0.080 g, 2.36·10⁻⁴ mol) in MeOH (20 mL) was added. After 24 h, MSNs were centrifuged, and the supernatant was collected to quantify the loading of the drug by UV-vis spectroscopy (354 nm). Then, the resulting MSNs were dispersed in a solution of DOX (21 mg, 3.6·10⁻⁵ mol) in MeOH (20 mL). Finally, after 48 h MSNs were washed with MeOH (three times) and H₂O (three times) until no red supernatant was obtained and then lyophilized. DOX and CPT loading content (%LC = [entrapped drug/nanoparticles weight] × 100) were quantified by UV-vis spectroscopy (354 and 490 nm, respectively) from the supernatant (the amount of CPT released to the supernatant during the pore capping was subtracted from the initial value of loaded drug (CPT@MSN-(NH₂)_i(CHO)_o)).

2.7. Release experiments of CPT@MSN-(NH₂)_i(PEG-DOX)_o

Release experiments were performed at pH = 7.4 (PBS buffer), pH = 6.5 (phosphate buffer, 0.2 M NaH₂PO₄/0.2 M Na₂HPO₄), pH = 5.5, 4.5, 4 (acetate buffer, 0.1 M NaAcO/0.1 M AcOH) and 1. For each release study, MSNs (10 mg) were dispersed by sonication (2 min) in the buffer solution (1.5 mL) and kept at 37 °C, while being stirred (100 rpm). At every designated interval, buffer solutions were taken out for analysis and centrifuged (12,000 rpm, 13 min). The solid residues were dispersed in fresh buffer solution (1.5 mL). The quantities of the drugs released into the buffer solution were measured by UV-vis absorption spectroscopy at 490 nm for DOX and 354 nm for CPT.

2.8. In vitro cytotoxicity

In vitro cytotoxicity was performed using the MTT assay in two tumor cell lines: HeLa and U-87 MG. Experiments were carried out in 96-well plates (0.1 mL/well) where 10,000 cells/well of the corresponding cell line were seeded using complete DMEM media (10% FBS, 1% glutamine, 1% penicillin/streptomycin). Twenty-four hours later, cells were incubated with MSNs for 24, 48 and 72 h at 37 °C and 5% CO₂. After a washing step with PBS, the MTT solution was added (0.5 mg/mL). Cells were incubated for 3 h at 37 °C and 5% CO₂, the MTT solution was removed, and formazan crystals were dissolved in 0.1 mL of DMSO. Finally, formazan absorbance was measured at 560 nm.

2.9. Confocal microscopy for cellular internalization

Uptake experiments were carried out on glass coverslips. 180,000 HeLa cells/well were seeded using complete DMEM media (10% FBS, 1% glutamine, and 1% penicillin/streptomycin). Twenty-four hours later, cells were incubated with CPT@MSN-hyd-PEG-hyd-DOX for 4 h at 37 °C and 5% CO₂. Then, cells were washed with PBS and fixed with 10% formalin. Finally, cells were observed in a fluorescence confocal microscopy (JEOL microscope model JEM-1400).

2.10. Bio-TEM

Two million HeLa cells were seeded onto a Petri dish in a complete DMEM medium and incubated at 37 °C with 5% CO₂ atmosphere for 24 h. Next, medium was removed and cells were incubated in new medium supplemented with CPT@MSN-hyd-PEG-hyd-DOX at 50 µg/ml for 4 h. Then, cells were fixed, first with 2% glutaraldehyde buffered in 0.1 M sodium cacodylate at room temperature for 1 h and afterward, with 2% osmium tetroxide containing 1.5% of potassium ferricyanide buffered in 0.1 M sodium cacodylate for 90 min at room temperature. Finally, samples were dehydrated in grading alcohols (70%, 90% and 100%) and included in Epon for at least 24 h at 60 °C. Thin slides were cut using microtome, deposited on copper grids, and stained with 5% uranyl acetate and 0.4% lead citrate. Observations were performed with transmission electron

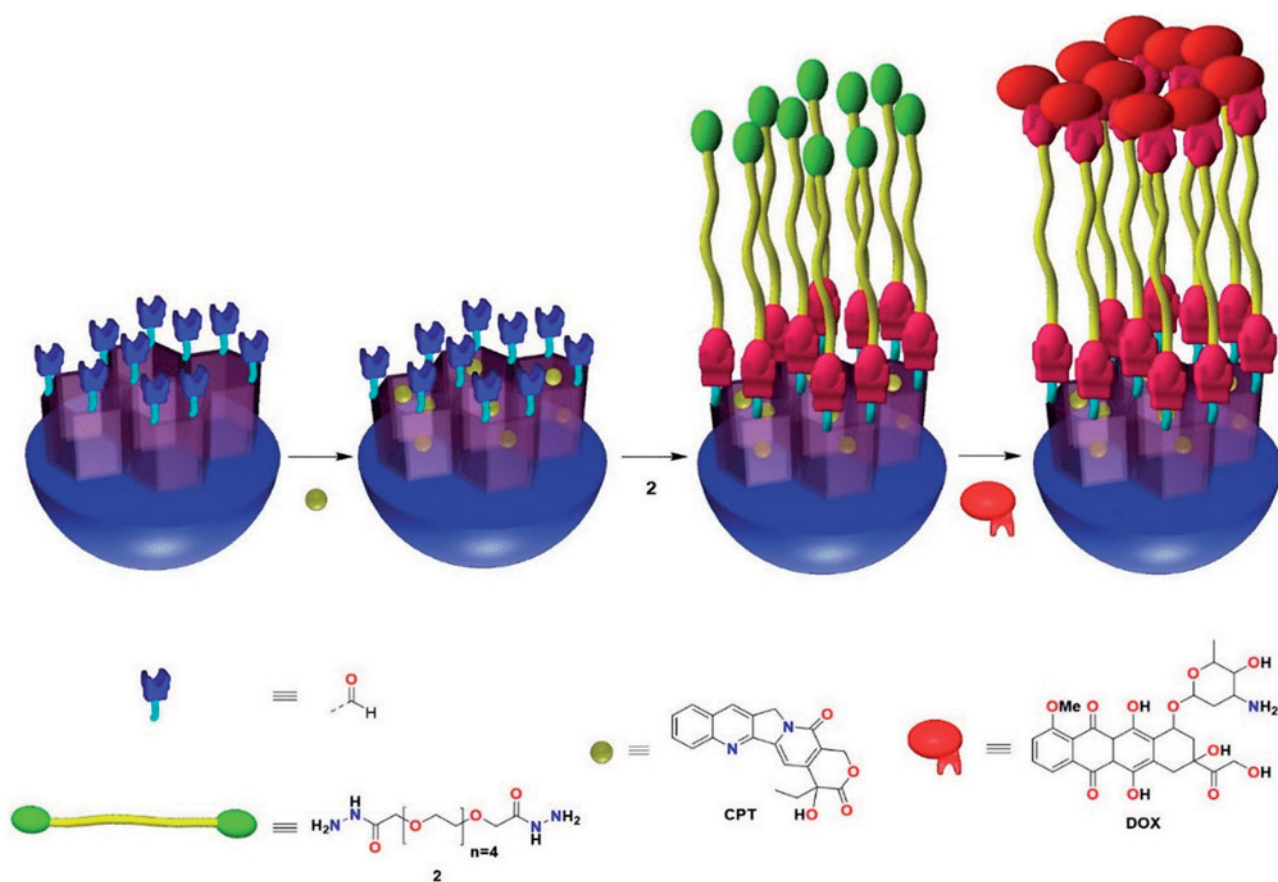


Figure 2. Preparation of the DDS.

microscope (JEOL microscope model JEM-1400) (Fischella et al., 2009).

2.11. FACS analysis

HeLa cells were seeded at a density of 20,000 cells/well in 96-well plates with complete DMEM media (10% FBS, 1% glutamine and 1% penicillin/streptomycin) and incubated at 37 °C, 5% CO₂ for 24 h. Then, CPT@MSN-hyd-PEG-hyd-DOX were added, and after a 4 h incubation period, cells were prepared for FACS analysis. Briefly, cells were washed with PBS, and harvested with 40 µl of trypsin per well. After a few minutes, 120 µl of complete DMEM were added, to stop trypsin reaction, and cells were fixed with 100 µl of paraformaldehyde 2%. Doxorubicine internalization was measured by flow cytometry analysis.

2.12. IncuCyte® S3 live-cell analysis

Uptake kinetics experiment were carried out in a 96-well plates (0.1 mL/well) where 15,000 HeLa cells/well were seeded using complete DMEM media (10% FBS, 1% glutamine and 1% penicillin/streptomycin). Twenty-four hours later, cells were incubated with CPT@MSN-hyd-PEG-hyd-DOX for 13.5 and 50.5 h at 37 °C and 5% CO₂. DOX release was monitored with IncuCyte® S3 live-cell analysis system, capturing live-cell images every 30 min.

3. Results and discussion

3.1. Preparation and characterization of the DDS

In order to build the proposed DDS, regioselectively functionalized amine-aldehyde MSNs were synthesized. While the inner amines will enhance drug loading and facilitate the release (Wang et al., 2009; Kamarudin et al., 2013; Natarajan & Selvaraj, 2014) the outer aldehyde moieties will react with the hydrazide groups of the cleavable-linker (Figure 2).

To the best of our knowledge, no examples of such amine-aldehyde MSNs have been described (Slowing et al., 2010). However, these bifunctional MSNs can be prepared regioselectively by chemical derivatization of the outer surface of mono-functionalized MSNs, with the pores blocked by the surfactant. Examples of application using this strategy have been reported by Ruiz-Hitzky et al. (de Juan & Ruiz-Hitzky, 2000) and Lin et al. (Huang et al., 2011).

Briefly, the preparation of amine-aldehyde MSNs requires two simple steps starting from MSN-(NH₂) CTAB, synthesized by a co-condensation procedure reported by Lo et al. (Cheng et al., 2009) (Scheme S1). First, MSN-(NH₂) CTAB were reacted for 24 h with 2-isothiocyanate-1,1-dimethoxyethane (**1**) in toluene (Scheme S2) (de Juan & Ruiz-Hitzky, 2000; Lee et al., 2010). This bifunctional acetal **1** can be easily synthesized from commercially available 2,2-dimethoxyethan-1-amine (Park et al., 2003). To effect the functionalization in a regioselective fashion, it is critical to carry out this reaction in toluene as a solvent. Under these conditions the surfactant

(CTAB) is preserved inside MSNs porous (Lee et al., 2010; Huang et al., 2011) as it can be inferred from inspection of the infrared spectrum of MSN-(NH₂)_i(Acet)_oCTAB (C-H stretch band of the tensioactive at 2900 cm⁻¹) (Figure S5) and BET analysis (Figure S6(a)).

Then, a treatment of the nanoparticles with NH₄NO₃ in EtOH removes the tensioactive yielding MSN-(NH₂)_i(Acet)_o. Finally, the acetal moiety was transformed into the aldehyde group, by acidic treatment affording the desired MSN-(NH₂)_i(CHO)_o. The formation of the aldehyde functionality is supported by the presence of two small absorption bands corresponding to the H-C=O stretch; both around 2990 cm⁻¹ (Figure S1), besides a weak band, corresponding to the C=O stretching, can be observed at 1730 cm⁻¹ overlapped with the bending vibration of water (1650 cm⁻¹) (Tian et al., 2017). The C=S asymmetric stretching mode, which corresponds to the thiourea formation, is observed at 1384 cm⁻¹ in the FT-IR spectrum (Figure S5). Additional prove of the successful functionalization is provided by the formation of the corresponding hydrazone when the nanoparticles are treated with 2,4-dinitrophenylhydrazine (aldehyde groups on the surface of the MSN ~1.3·10⁻⁷ mol mg⁻¹ MSN) (Scheme S3 and Figure S2).

The bifunctionalized amino-aldehyde MSNs were characterized by standard techniques (DLS, TEM, BET and powder XRD analysis). These analyses suggest that the introduction of the aldehyde group does not erode the structural features of the MSNs. As shown in Figure S4(b), MSN-(NH₂)_i(CHO)_o are round shaped with a diameter around 100 nm. No significant size differences were obtained between initial aminated nanoparticles (MSNs-(NH₂)) and bifunctionalized amino-aldehyde nanoparticles (MSNs-(NH₂)_i(CHO)_o) (Table S1).

Powder XDR analysis indicates highly ordered structures with intense (100) reflection peaks corresponding to lattice spacing in the range of 4.1–4.2 nm, which is attributed to two-dimensional (2D) long-range ordered structure (Figure S3). N₂ adsorption/desorption measurements of MSN-(NH₂)_i(CHO)_o showed type IV isotherms, which display clear H1 hysteresis loop characteristic of mesoporous materials. BET surface areas are over 1007 m²·g⁻¹ for MSN-(NH₂) and 990 m²·g⁻¹ for MSN-(NH₂)_i(CHO)_o (Figure S6(a)). Furthermore, the pore volume for MSN-(NH₂)_i(CHO)_o was 0.56 cm³·g⁻¹ and 0.67 cm³·g⁻¹ for reference MSN-(NH₂) (Table S2). These MSN-(NH₂)_i(CHO)_o presents a very narrow pore size distribution centered at 2.4 nm (Figure S6(b)).

Next, the preparation of the requisite blocking linker was carried out. It is proposed the use of a dihydrazide–polyethylene glycol chain (Huan et al., 2012; Brinkhuis et al., 2013; Wang et al., 2014a) with the purpose of not only sealing the MSNs pores (Lee et al., 2010; Agostini et al. 2012b; Aznar et al., 2012; El Sayed et al., 2015) but also enhance the hydrophilicity of the nanoparticle in order to reduce the phagocytosis of macrophages (Figure 2) (Li et al., 2014; El Sayed et al., 2015). According to the literature (Agostini et al., 2012b; Aznar et al., 2012; El Sayed et al., 2015) functionalized tetraethylene glycol chains have shown to be able to block quite efficiently the porous entrance of MSNs. Hence, 3,6,9,12,15-pentaoxaheptadecanedihydrazide (**2**) was prepared. This difunctional PEG can be synthesized from

commercially available tetraethylene glycol in two steps according to reported procedures with an overall yield of 47% (Scheme S4) (Wittmann et al., 1998; Zhang et al., 2015).

With the dihydrazide linker and the amine-aldehyde MSNs in hand, the nano-vehicle was prepared (Figure 2). First, CPT was loaded inside amine-aldehyde MSNs pores. Several methods using different solvent mixtures were tested, among them MeOH (Agostini et al., 2012b) CHCl₃/MeOH (Mondragon et al. 2014) ACN/EtOH (Agostini et al., 2012b) DMSO (Muhammad et al., 2014) and DMF (Li et al., 2013). However, in our hands, the mixture CHCl₃/MeOH allowed the most satisfactory loading (Lu et al., 2007). Maximum loading for CPT, assessed either by absorption spectroscopy or by OEA, was obtained as 1.36·10⁻⁸ mol CPT·mg⁻¹ MSN, which corresponds to 3.1%. This loading is comparable to reported values in similar systems, which range from 2% to 5% (Li et al., 2013). Then, an excess of 3,6,9,12,15-pentaoxaheptadecanedihydrazide (**2**) was added to the solution in order to promote aldehyde MSNs reaction with only one of the terminal moieties of the linker. Afterward, the addition of DOX to the solution gave CPT@MSN-hyd-PEG-hyd-DOX (Figure 2). The excess quantities of CPT, DOX and dihydrazide PEG **2** were removed by washing several times with MeOH and H₂O. Finally, the nanoparticles were lyophilized. All the steps of this procedure were carried out smoothly at room temperature. Approximately, 7.06·10⁻⁷ mol DOX·mg⁻¹ MSN were incorporated to the MSNs, which corresponds to 25%. In comparison with other hydrazone linkage systems, the values of DOX loading that have been obtained are excellent (Lee et al., 2010, 2011; Fan et al., 2011; Li et al., 2013). The geometry (round shape, diameter = 100 nm) and structural integrity of the CPT@MSN-hyd-PEG-hyd-DOX were evaluated by TEM (Figure S4(c)). The images confirm that the loading process had not eroded the nanoparticles. As expected, DOX molecules on the surface of the nanoparticle induce a highly positive ζ-potential value (+20.1 mV) due to the presence of an amino sugar in the structure of the drug. This cationic character of the particle surface could enhance the cellular uptake and minimize the self-aggregation. As shown in Figure S4(c) the mesopores of CPT@MSN-hyd-PEG-hyd-DOX were masked due to the drug loading and chemical modification of the surface.

3.2. Controlled drug release

The release profiles of CPT and DOX from CPT@MSN-hyd-PEG-hyd-DOX were studied by UV–vis absorption spectroscopy at pH values of 1.0, 4.0, 4.5, 5.5, 6.5, and 7.4 (Figure 3). At pH = 1 it is measured the total amount of drug that can be released under acid conditions. From this measurements, it can be concluded that under normal physiological conditions (pH = 7.4) DOX and CPT release is virtually negligible, indicating that the DDS have a well protection from the drug releasing in normal tissues, which is essential given the high toxicity of these drugs (Li et al., 2013; Muhammad et al., 2014). It is suggested that DOX plays a key role in the sealing of the nanoparticle, since its presence would lead to rigid tetraethylene glycol chains, due to the bulkiness of the

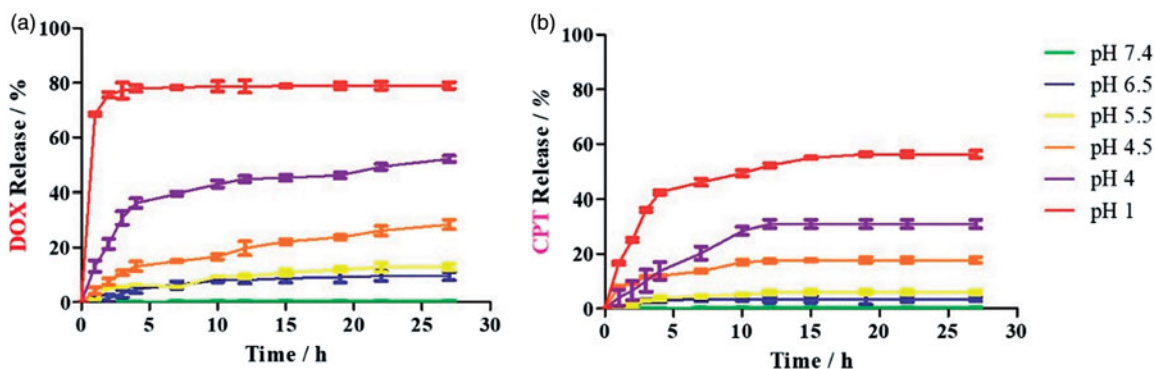


Figure 3. (a) DOX and (b) CPT release profile of CPT@MSN-hyd-PEG-hyd-DOX at different pH values under stirring at 100 rpm and at $t = 37^{\circ}\text{C}$.

molecule and the repulsive interaction between ammonium groups, providing an efficient pore closure.

However, under acidic conditions a burst release of DOX takes place, with approximately 80%, 45%, 25% and 10% of the drug released within 20 h at pH 1.0, 4.0, 4.5 and 5.5, respectively (Figure 3). It is hypothesized that this rapid release coincides with the cleavage of the hydrazone bond. The role of pH in the release has been studied and demonstrated (Figures S9 and S10). Finally, from $t = 5$ h the rate of release is slower albeit sustained. By contrast, CPT@MSN-hyd-PEG-hyd-DOX under the same conditions exhibit a sustained CPT release for more than 10 h, which might be ascribed to the physical absorption of the drug inside the nanochannels (Luo et al., 2013). The smooth release pattern observed for CPT can be especially beneficial for combination therapy (Cao et al., 2014; Xu et al., 2015b; Kennedy et al., 2016).

3.3. Intracellular uptake

Cellular uptake and drug release were investigated by confocal laser scanning microscopy (CLSM). To do so, a homogeneous suspension of CPT@MSN-hyd-PEG-hyd-DOX ($50\ \mu\text{g}\ \text{MSN}\cdot\text{mL}^{-1}$) in complete Dulbecco's modified eagle medium (DMEM) was added to HeLa cells (Xu et al., 2015a). After four hours of incubation, cell images (Figure 4(b,c)) show blue and red fluorescence in cell bodies, suggesting an efficient uptake and subsequent release of both drugs from the nanovehicle. Figure 4(d) illustrates merged fluorescence of DOX and CPT, indicating the co-delivery of both drugs into the cells (Park et al., 2003; Li et al., 2013; Muhammad et al., 2014). As expected, a significant red fluorescence signal is detected in the nucleus of the cells (Figure 4(c), yellow arrows), which is in agreement with the preferential accumulation of DOX in this organelle. Thus, these results demonstrate that after the uptake of the nano-vehicle DOX was released by hydrolysis of the hydrazone bonds in response to the acidic environment found in the cell. By contrast, blue fluorescence of CPT, which has been released by diffusion from the pores of the nanoparticle, was only detected in the cytoplasmic matrix (Figure 4(b)).

Further confirmation of this efficient uptake of the DDS and release of DOX was obtained by flow cytometry analysis (FACS analysis) (Figure S11). It is hypothesized that the uptake of CPT@MSN-hyd-PEG-hyd-DOX is influenced and enhanced by the presence of at least partially protonated

amino groups bonded to the sugar moiety of DOX, which is attached to the surface of the nanoparticle (Luo et al., 2014). This hypothesis is consistent with the highly positive ζ -potential value measured for CPT@MSN-hyd-PEG-hyd-DOX.

Furthermore, Bio-TEM was used to verify the intracellular uptake of individual nanoparticles (1) (Figure 5). As it can be seen in Figure 5(a), the endocytosed nanocarrier was principally accumulated within endosomes and/or lysosomes in the cytosol (2) of the cell. The confinement of the nanoparticles in such organelles would explain the acid hydrolysis of the hydrazone bonds, which is responsible for the release of the drugs from the DDS. Although many groups of nanoparticles could be seen distributed around the nucleus (3), no nanoparticles appeared to be able to enter into this organelle. This is in agreement with reports that indicate the impossibility of nanoparticles with a diameter over 100 nm to cross the nuclear membrane. Figure 5(b), shows a cluster of nanoparticles that have escaped from the endosome, probably via cellular 'sponge effects', and entered into the cytoplasm. It is worth noting that the internalized nanoparticles still kept their spherical shape and structural integrity. Interestingly, in some micrographs it was possible to observe characteristic ruffles of the plasma suggesting an endocytosis process (Figure 5(c)).

3.4. Cytotoxicity

To assess the cytotoxicity and therapeutic efficiency caused by the co-delivery of the two drugs, MTT assays in HeLa and human glioblastoma astrocytoma (U-87 MG) cell lines were carried out (Xu et al., 2015a). Therefore, two control nanoparticles MSN-(NH₂), MSN-(NH₂)_i(CHO)_o (which represents the final nanoparticle after the release of the two drugs without the presence of the PEG chain), and drug loaded nanocarriers CPT@MSN-hyd-PEG-hyd, MSN-hyd-PEG-hyd-DOX and CPT@MSN-hyd-PEG-hyd-DOX at 1, 5, 25, 50 and 100 $\mu\text{g}\ \text{MSN}\cdot\text{mL}^{-1}$ were added and incubated with the cells for 72 h. The results of these assays are shown in Figure 6.

The viability assays revealed that control nanoparticles had no obvious toxicity on HeLa or U-87 MG cells in a range of concentrations from 1 to 100 $\mu\text{g}\ \text{mL}^{-1}$ (Figure 6). Interestingly, DDS without any drug (MSN-(NH₂)_i(CHO)_o) show viabilities higher than 90%, thus meaning that all the cytotoxic effect seen with CPT@MSN-hyd-PEG-hyd-DOX was solely

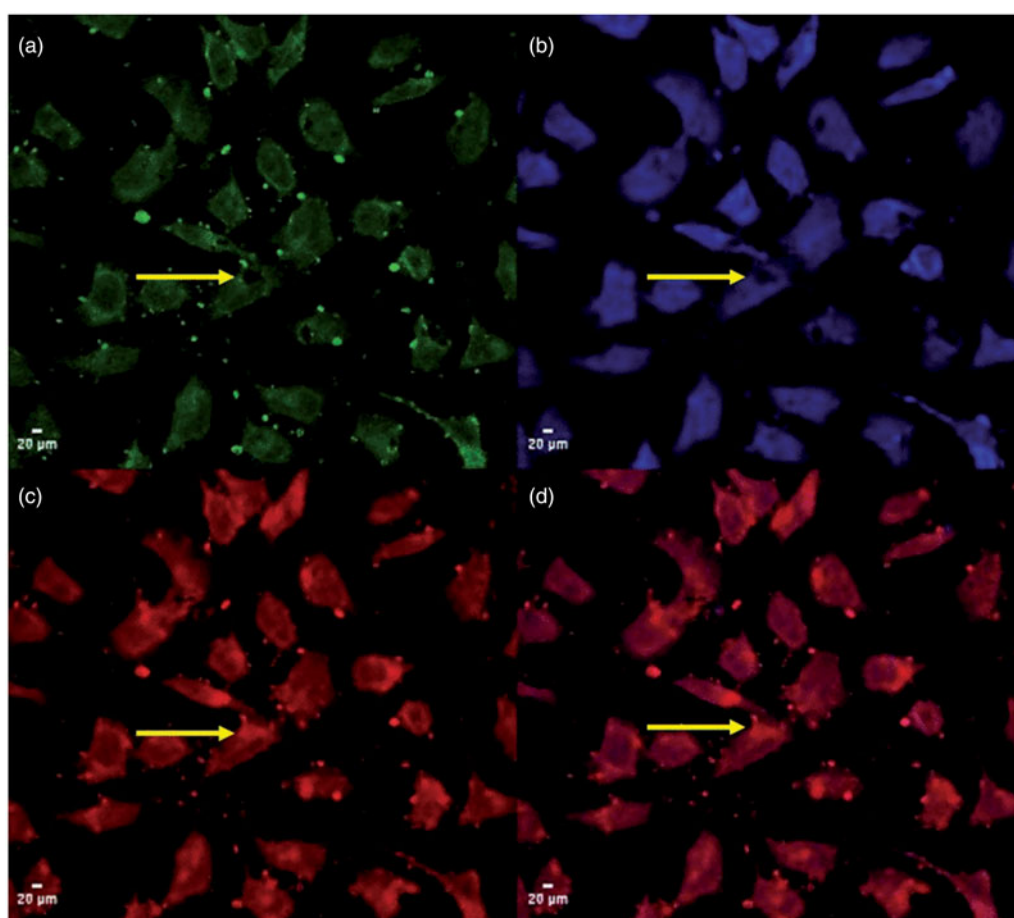


Figure 4. CLSM images of the uptake of CPT@MSN-hyd-PEG-hyd-DOX scale bar 20 μm . (a) corresponds to fluorescein diacetate (FDA) fluorescence, (b) CPT fluorescence, (c) DOX fluorescence and (d) DOX and CPT merged images.

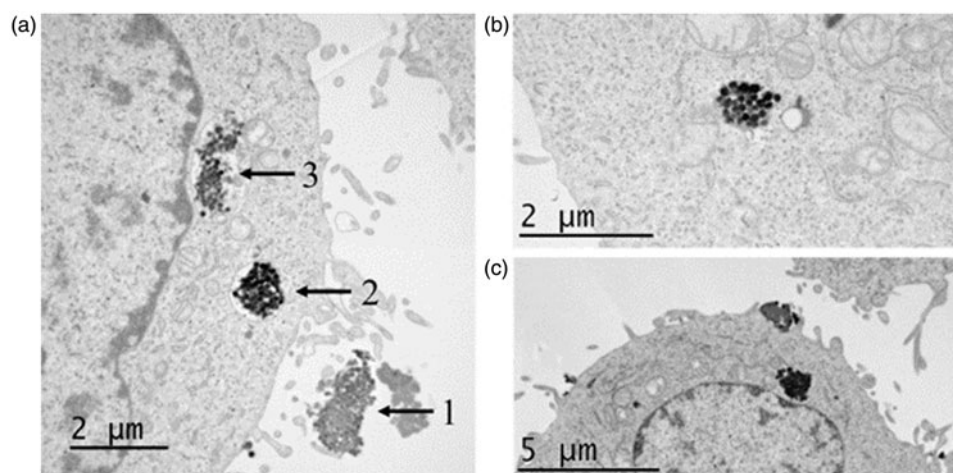


Figure 5. (a) Transmission electron microscopy (TEM) images of HeLa cells incubated for 4 h with 50 $\mu\text{g mL}^{-1}$ of CPT@MSN-hyd-PEG-hyd-DOX (b) a cluster of nanoparticles that have escaped from the endosome (c) internalization of the nanoparticles.

due to the DOX and CPT released from the DDS. Therefore, these DDS can be regarded as biocompatible.

By contrast, DOX loaded MSN-hyd-PEG-hyd-DOX, reduces the viability of HeLa cells to 6% at doses of 100 $\mu\text{g}\cdot\text{mL}^{-1}$. For this system, the half-maximal inhibitory concentration (IC_{50}) was 5 $\mu\text{g}\cdot\text{mL}^{-1}$. This value is in the same order of magnitude of that of free DOX ($\text{IC}_{50} = 1.2 \mu\text{g}\cdot\text{mL}^{-1}$) (Huang et al., 2007). But more importantly, it was found that the effect of the

CPT/DOX loaded nano-carrier CPT@MSN-hyd-PEG-hyd-DOX on the HeLa cells was an increase in the cell death compared with the nanoparticles loaded only with DOX (Figure 6(a)). For instance, cell viability at 5 $\mu\text{g}\cdot\text{mL}^{-1}$ decreases from 50% (DOX) to a 28% (CPT/DOX). Interestingly, the combination effect of both drugs increases with time. Thus, at 24 h the effect of the combined treatment on the cell death is essentially the same that is displayed in the presence of DOX

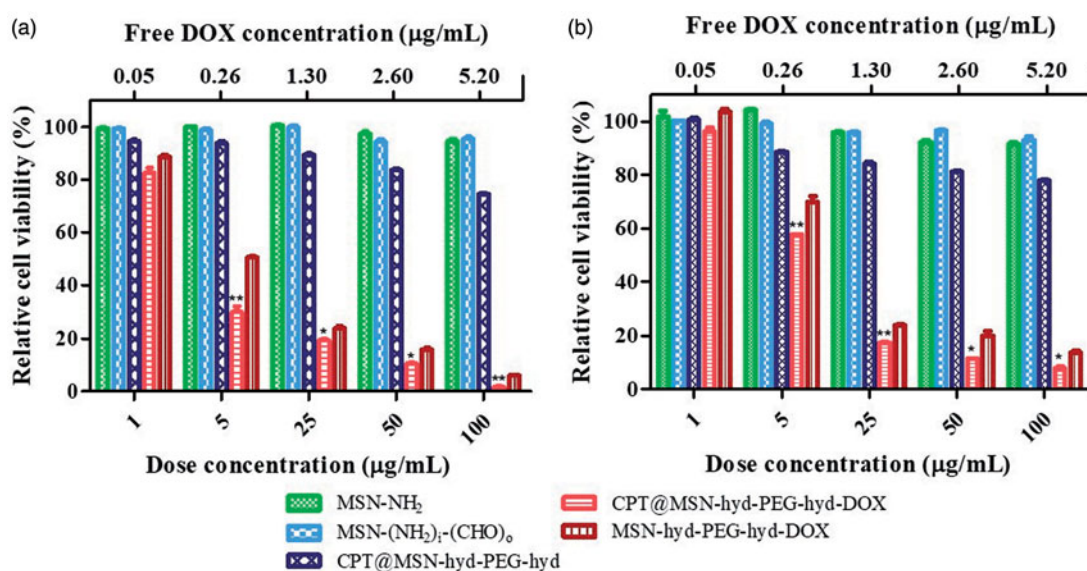


Figure 6. Cell viability of (a) HeLa cells and (b) U-87 MG cells incubated with MSN-(NH₂)_i, MSN-(NH₂)_i-(CHO)_o, MSN-hyd-PEG-hyd-DOX, CPT@MSN-hyd-PEG-hyd and CPT@MSN-hyd-PEG-hyd-DOX. Data represented as mean ± SD, **p* < .05 and ***p* < .01. The concentration of free DOX is the released drug at pH = 5.5.

alone (Figure S12). However, at 48 h and more clearly at 72 h, cell viabilities decrease significantly. This delayed effect of CPT can be ascribed to the slow release of the drug from the pores and its mechanism of action. All these observations are consistent with a combination effect between these two drugs and proves the successful co-delivery of DOX and CPT to the cells (Muhammad et al., 2014; Li et al., 2015b).

The calculated value of IC₅₀ for CPT@MSN-hyd-PEG-hyd-DOX is 1.88 µg·mL⁻¹ and is equivalent to the release of 0.09 µg·mL⁻¹ of free DOX. The later value was calculated as the release of the drug at pH = 5.5, which is the average pH found in late-endosomes and lysosomes. At the same pH conditions, the calculated CI (combination index) value is 0.14 (at IC₅₀), which is consistent with a synergistic interaction of the drugs.

To gain insight into the uptake of CPT@MSN-hyd-PEG-hyd-DOX into HeLa cells the kinetics of the release of DOX were studied using an IncuCyte[®] S3 live-cell analysis system. Thus, monitoring DOX fluorescence inside the cells revealed that after an incubation period of 3–4 h, an increase of DOX content took place (Figure S14). This initial period is ascribed to the uptake of the nanoparticle by the cell. Afterwards, a sustained increase of DOX fluorescence during 14 h was observed and after a period of 25 h, cell death could be easily detected by inspection of the micrographs (Figure S15).

Additionally, cell death assays with cell line U-87 MG were carried out (Figure 6(b)). The effect on the viability of the cells was less marked than with HeLa cells. However, the combination effect of the two drug was also observed, for instance, from comparison of cell viability at 5 µg/mL in the presence of nanoparticles loaded with DOX alone (MSN-hyd-PEG-hyd-DOX) or the combination of both drugs CPT/DOX (CPT@MSN-hyd-PEG-hyd-DOX). These values were 70% and 57%, respectively. As reference, at the same concentration, HeLa cells showed values of 50% and 28% of viability indicating a higher sensitivity to these treatments. As it was observed with HeLa cells, the effects of the combined treatment (CPT/DOX) are more significant at 72 h than at 24 h

(Figure S13). The calculated value of IC₅₀ for CPT@MSN-hyd-PEG-hyd-DOX is 4.22 µg·mL⁻¹, and the corresponding CI was 0.32. Again, a synergistic effect on combining both drugs takes place.

4. Conclusions

In summary, a pH-triggered nano-vehicle with regioselectively bifunctionalized MSN-(NH₂)_i-(CHO)_o nanoparticles for the dual release of DOX/CPT has been prepared. The synthesis of the carrier consists of three steps: (1) preparation of MSN-(NH₂) CTAB, (2) synthesis of MSN-(NH₂)_i-(CHO)_o and (3) loading of CPT followed by capping with dihydrazide PEG 2 and DOX in a one-pot procedure. From a practical standpoint, it is noteworthy the succinct preparation of the carrier avoiding multi-step syntheses or the chemical derivatization to the drugs. *In vitro* tests show that CPT@MSN-hyd-PEG-hyd-DOX can be efficiently internalized into HeLa and U-87 MG cells. Moreover, the nanoparticles can deliver CPT and DOX leading to an acidity-activated synergistic chemotherapy. The release of DOX or CPT at physiological pH is negligible reducing the intrinsic toxicity of the treatment. Currently, the preparation of decorated DDS with receptor-specific ligands is undertaken in our laboratories to enhance their selectivity.

Acknowledgements

M.C.L and G.M.E are grateful to IQS for financial support. We would like to thank Generalitat de Catalunya for the consolidated Research Group Grant (SGR) 1170 to GEMAT. The authors acknowledge the technical assistance of Dr. Alejandro Sánchez-Chardi and Ms. Nuria Barba Bosch from the Microscopy Facility of the Universitat Autònoma de Barcelona (UAB).

Disclosure statement

The authors declare no competing financial interest.

ORCID

Salvador Borrós  <http://orcid.org/0000-0002-4003-0381>
 David Sánchez-García  <http://orcid.org/0000-0002-3936-9329>

References

- Agostini A, Mondragón L, Coll C, et al. (2012a). Dual enzyme-triggered controlled release on capped nanometric silica mesoporous supports. *ChemistryOpen* 1:17–20.
- Agostini A, Mondragón L, Pascual L, et al. (2012b). Design of enzyme-mediated controlled release systems based on silica mesoporous supports capped with ester-glycol groups. *Langmuir* 28:14766–76.
- Argyó C, Weiss V, Bräuchle C, Bein T. (2014). Multifunctional mesoporous silica nanoparticles as a universal platform for drug delivery. *Chem Mater* 26:435–51.
- Aznar E, Sancenón F, Marcos MD, et al. (2012). Delivery modulation in silica mesoporous supports via alkyl chain pore outlet decoration. *Langmuir* 28:2986–96.
- Brinkhuis RP, de Graaf F, Hansen MB, et al. (2013). Dynamically functionalized polymersomes via hydrazine exchange. *Polym Chem* 4:1345–50.
- Camacho KM, Kumar S, Menegatti S, et al. (2015). Synergistic antitumor activity of camptothecin–doxorubicin combinations and their conjugates with hyaluronic acid. *J Control Release* 210:198–207.
- Cao Y, Wang B, Wang Y, Lou D. (2014). Polymer-controlled core–shell nanoparticles: a novel strategy for sequential drug release. *RSC Adv* 4:30430.
- Cheng S-H, Lee C-H, Yang C-S, et al. (2009). Mesoporous silica nanoparticles functionalized with an oxygen-sensing probe for cell photodynamic therapy: potential cancer theranostics. *J Mater Chem* 19:1252.
- Choi KY, Liu G, Lee S, Chen X. (2012). Theranostic nanoplateforms for simultaneous cancer imaging and therapy: current approaches and future perspectives. *Nanoscale* 4:330–42.
- Coti KK, Belowich ME, Liong M, et al. (2009). Mechanised nanoparticles for drug delivery. *Nanoscale* 1:16–39.
- de Juan F, Ruiz-Hitzky E. (2000). Selective functionalization of mesoporous silica. *Adv Mater* 12:430–2.
- El Sayed S, Gimenez C, Aznar E, et al. (2015). Highly selective and sensitive detection of glutathione using mesoporous silica nanoparticles capped with disulfide-containing oligo(ethylene glycol) chains. *Org Biomol Chem* 13:1017–21.
- Fan J, Fang G, Wang X, et al. (2011). Targeted anticancer prodrug with mesoporous silica nanoparticles as vehicles. *Nanotechnology* 22:455102.
- Fischella M, Dabboue H, Bhattacharyya S, et al. (2009). Mesoporous silica nanoparticles enhance MTT formazan exocytosis in HeLa cells and astrocytes. *Toxicol. in Vitro* 23:697–703.
- Gao W, Chan JM, Farokhzad OC. (2010). pH-responsive nanoparticles for drug delivery. *Mol Pharmaceutics* 7:1913–20.
- Huan M, Zhang B, Teng Z, et al. (2012). In vitro and in vivo antitumor activity of a novel pH-activated polymeric drug delivery system for doxorubicin. *PLoS One* 7:e44116.
- Huang CK, Lo CL, Chen HH, Hsiue GH. (2007). Multifunctional micelles for cancer cell targeting, distribution imaging, and anticancer drug delivery. *Adv Funct Mater* 17:2291–7.
- Huang Y, Xu S, Lin VSY. (2011). Bifunctionalized mesoporous materials with site-separated brønsted acids and bases: catalyst for a two-step reaction sequence. *Angew Chem Int Ed* 50:661–4.
- Kamarudin NHN, Jalil AA, Triwahyono S, et al. (2013). Role of 3-aminopropyltriethoxysilane in the preparation of mesoporous silica nanoparticles for ibuprofen delivery: effect on physicochemical properties. *Micropor Mesopor Mat* 180:235–41.
- Kar M, Tiwari N, Tiwari M, et al. (2013). Poly-L-arginine grafted silica mesoporous nanoparticles for enhanced cellular uptake and their application in DNA delivery and controlled drug release. *Part Part Syst Charact* 30:166–79.
- Kennedy S, Hu J, Kearney C, et al. (2016). Sequential release of nanoparticle payloads from ultrasonically burstable capsules. *Biomaterials* 75:91–101.
- Khung YL, Narducci D. (2015). Surface modification strategies on mesoporous silica nanoparticles for anti-biofouling zwitterionic film grafting. *Adv Colloid Interface Sci* 226:166–86.
- Kim Y-H, Lee JK, Kim B, et al. (2013). Combination therapy of cilengitide with belotecan against experimental glioblastoma. *Int J Cancer* 133:749–56.
- Lee C-H, Cheng SH, Huang IP, et al. (2010). Intracellular pH-responsive mesoporous silica nanoparticles for the controlled release of anticancer chemotherapeutics. *Angew Chem Int Ed Engl* 49: 8214–9.
- Lee JE, Lee DJ, Lee N, et al. (2011). Multifunctional mesoporous silica nanocomposite nanoparticles for pH controlled drug release and dual modal imaging. *J Mater Chem* 21:16869.
- Li Z, Barnes JC, Bosoy A, et al. (2012). Mesoporous silica nanoparticles in biomedical applications. *Chem Soc Rev* 41:2590–605.
- Li Z, Li H, Liu L, et al. (2015a). A pH-sensitive nanocarrier for co-delivery of doxorubicin and camptothecin to enhance chemotherapeutic efficacy and overcome multidrug resistance in vitro. *RSC Adv* 5:77097–105.
- Li ZY, Liu Y, Wang XQ, et al. (2013). One-pot construction of functional mesoporous silica nanoparticles for the tumor-acidity-activated synergistic chemotherapy of glioblastoma. *ACS Appl Mater Interfaces* 5:7995–8001.
- Li QL, Sun Y, Sun YL, et al. (2014). Mesoporous silica nanoparticles coated by layer-by-layer self-assembly using cucurbit[7]uril for in vitro and in vivo anticancer drug release. *Chem Mater* 26:6418–31.
- Li Q-L, Xu S-H, Zhou H, et al. (2015b). pH and glutathione dual-responsive dynamic cross-linked supramolecular network on mesoporous silica nanoparticles for controlled anticancer drug release. *ACS Appl Mater Interfaces* 7:28656–64.
- Lu J, Liong M, Zink JL, Tamanoi F. (2007). Mesoporous silica nanoparticles as a delivery system for hydrophobic anticancer drugs. *Small* 3:1341–6.
- Luo G-F, Chen W-H, Liu Y, et al. (2013). Charge-reversal plug gate nanovalves on peptide-functionalized mesoporous silica nanoparticles for targeted drug delivery. *J Mater Chem B* 1:5723.
- Luo GF, Chen WH, Liu Y, et al. (2014). Multifunctional enveloped mesoporous silica nanoparticles for subcellular co-delivery of drug and therapeutic peptide. *Sci Rep* 4:6064.
- Mai WX, Meng H. (2013). Mesoporous silica nanoparticles: a multifunctional nano therapeutic system. *Integr Biol* 5:19–28.
- Mamaeva V, Sahlgren C, Linden M. (2013). Mesoporous silica nanoparticles in medicine – recent advances. *Adv Drug Deliv Rev* 65:689–702.
- Martínez-Carmona M, Colilla M, Vallet-Regí M. (2015). Smart mesoporous nanomaterials for antitumor therapy. *Nanomaterials* 5:1906.
- Miles D, von Minckwitz G, Seidman AD. (2002). Combination versus sequential single-agent therapy in metastatic breast cancer. *Oncologist* 7(suppl 6):13–9.
- Mondragon L, Mas N, Ferragud V, et al. (2014). Enzyme-responsive intracellular-controlled release using silica mesoporous nanoparticles capped with ϵ -poly-L-lysine. *Chem Eur J* 20:5271–81.
- Muhammad F, Guo M, Wang A, et al. (2014). Responsive delivery of drug cocktail via mesoporous silica nanolamps. *J Colloid Interface Sci* 434:1–8.
- Natarajan SK, Selvaraj S. (2014). Mesoporous silica nanoparticles: importance of surface modifications and its role in drug delivery. *RSC Adv* 4:14328.
- Nonnenmacher L, Westhoff M-A, Fulda S, et al. (2015). RIST: a potent new combination therapy for glioblastoma. *Int J Cancer* 136: E173–E187.
- Park S, Hayes BL, Marankan F, et al. (2003). Regioselective covalent modification of hemoglobin in search of antisickling agents. *J Med Chem* 46:936–53.
- Pavillard V, Kherfellah D, Richard S, et al. (2001). Effects of the combination of camptothecin and doxorubicin or etoposide on rat glioma cells and camptothecin-resistant variants. *Br J Cancer* 85:1077–83.

- Rosenholm JM, Mamaeva V, Sahlgren C, Lindén M. (2011). Nanoparticles in targeted cancer therapy: mesoporous silica nanoparticles entering preclinical development stage. *Nanomedicine (Lond)* 7:111–20.
- Rosenholm J, Sahlgren C, Linden M. (2010). Cancer-cell targeting and cell-specific delivery by mesoporous silica nanoparticles. *J Mater Chem* 20:2707–13.
- Schmid B, Chung D-E, Warnecke A, et al. (2007). Albumin-binding prodrugs of camptothecin and doxorubicin with an Ala-Leu-Ala-Leu-linker that are cleaved by cathepsin B: synthesis and antitumor efficacy. *Bioconjugate Chem* 18:702–16.
- Shah MA, Schwartz GK. (2000). The relevance of drug sequence in combination chemotherapy. *Drug Resist Updat* 3:335–56.
- Shen Y, Jin E, Zhang B, et al. (2010). Prodrugs forming high drug loading multifunctional nanocapsules for intracellular cancer drug delivery. *J Am Chem Soc* 132:4259–65.
- Siegel RL, Miller KD, Jemal A. (2015). Cancer statistics, 2015. *CA Cancer J Clin* 65:5–29.
- Slowing II, Vivero-Escoto JL, Trewyn BG, Lin VSY. (2010). Mesoporous silica nanoparticles: structural design and applications. *J Mater Chem* 20:7924.
- Song N, Yang Y-W. (2015). Molecular and supramolecular switches on mesoporous silica nanoparticles. *Chem Soc Rev* 44:3474–504.
- Tian Z, Xu Y, Zhu Y. (2017). Aldehyde-functionalized dendritic mesoporous silica nanoparticles as potential nanocarriers for pH-responsive protein drug delivery. *Mater Sci Eng C Mater Biol Appl* 71:452–9.
- Trewyn BG, Slowing II, Giri S, et al. (2007). Synthesis and functionalization of a mesoporous silica nanoparticle based on the sol-gel process and applications in controlled release. *Acc Chem Res* 40:846–53.
- Vivero-Escoto JL, Slowing II, Trewyn BG, Lin VS. (2010). Mesoporous silica nanoparticles for intracellular controlled drug delivery. *Small* 6:1952–67.
- Wang AZ, Langer R, Farokhzad OC. (2012). Nanoparticle delivery of cancer drugs. *Annu Rev Med* 63:185–98.
- Wang G, Otuonye AN, Blair EA, et al. (2009). Functionalized mesoporous materials for adsorption and release of different drug molecules: a comparative study. *J Solid State Chem* 182:1649–60.
- Wang S, Wang H, Liu Z, et al. (2014a). Smart pH- and reduction-dual-responsive folate-PEG-coated polymeric lipid vesicles for tumor-triggered targeted drug delivery. *Nanoscale* 6:7635–42.
- Wang W, Wen Y, Xu L, et al. (2014b). A selective release system based on dual-drug-loaded mesoporous silica for nanoparticle-assisted combination therapy. *Chem Eur J* 20:7796–802.
- Wittmann V, Takayama S, Gong KW, et al. (1998). Ligand recognition by E- and P-selectin: chemoenzymatic synthesis and inhibitory activity of bivalent Sialyl Lewis x derivatives and Sialyl Lewis x carboxylic acids. *J Org Chem* 63:5137–43.
- Xu Z, Liu S, Kang Y, Wang M. (2015a). Glutathione- and pH-responsive nonporous silica prodrug nanoparticles for controlled release and cancer therapy. *Nanoscale* 7:5859–68.
- Xu W, Thapa R, Liu D, Nissinen T, Granroth S, Narvanen A, Suvanto M, Santos HA, Lehto VP. (2015b). Smart porous silicon nanoparticles with polymeric coatings for sequential combination therapy. *Mol Pharmaceutics* 12:4038–47.
- Yang KN, Zhang CQ, Wang W, et al. (2014). pH-responsive mesoporous silica nanoparticles employed in controlled drug delivery systems for cancer treatment. *Cancer Biol. Med* 11:34–43.
- Zhang Y-C, Zhang D-W, Wang H, et al. (2015). Bipyridinium radical cation dimerization-driven polymeric pleated foldamers and a homoduplex that undergo ion-tuned interconversion. *Polym Chem* 6:4404–8.
- Zhao Y, Trewyn BG, Slowing II, Lin VS. (2009). Mesoporous silica nanoparticle-based double drug delivery system for glucose-responsive controlled release of insulin and cyclic AMP. *J Am Chem Soc* 131:8398–400.
- Zhou S, Sha H, Ke X, et al. (2015). Combination drug release of smart cyclodextrin-gated mesoporous silica nanovehicles. *Chem Commun* 51:7203–6.